Coexistence of vortex and corner zero-energy excitations in the 2D second-order topological superconductor

A. D. Fedoseev* and A. O. Zlotnikov†

Kirensky Institute of Physics, Federal Research Center KSC SB RAS, 660036 Krasnoyarsk, Russia

(Dated: November 25, 2024)

While the appearance of vortex zero-energy modes in first-order 2D topological superconductors is well known, their possibility to appear in higher-order topological phase of 2D systems has not been completely uncovered yet. Here we demonstrate the coexistence of the zero-energy vortex modes and topological corner modes in the model of 2D second-order topological superconductor. The model describes an interface between a normal layer supporting the topological insulating phase and a superconducting layer, for which different symmetries of the superconducting order parameter are considered: $s_\pm$-wave, $d_{x^2-y^2}$-wave, as well as $s + d_{x^2-y^2}$-wave. The conditions of coexistence of vortex and corner zero-energy excitations are established and the interaction of vortex modes with the edge and topological corner modes is studied.

I. INTRODUCTION

The development of the concept of topologically non-trivial systems has led in recent years to an active study of higher-order topological insulators and superconductors (HOTSCs) [1–6]. The spectrum of their both bulk and edge states has a gap. In turn, topologically protected gapless excitations arise, being localized at the boundaries of higher orders, i.e. at corners (corners and hinges) in 2D (3D) systems [7]. It is important to note that in case of 2D HOTSCs such states are Majorana corner modes (MCMs) which possess zero energy and can be used for the braiding procedure [8–10] as obey non-Abelian exchange statistics [11, 12], which can be used for realization of quantum computation [13].

It is well known that Majorana zero modes formed near the boundaries and Majorana zero modes localized at the vortex cores correspond to each other in first-order topological superconductors (FOTSCs) [14]. It is supposed that existence of one type of such excitations (edge or vortex) guarantees presence of excitations of the other type in the same system. The interplay between Majorana edge and vortex states has been extensively studied in different FOTSCs, such as triplet $p_x + ip_y$-wave superconductors [15, 16], superconducting structures with spin-orbit interaction [17, 18], topological insulator and superconductor heterostructures [19–21], spin-singlet superconductors with noncollinear spin ordering [22] and others. Considering the vector-potential of the magnetic field modify the interaction between vortex and edge modes, since the second Majorana mode (called "exterior") is localized in this case on the characteristic magnetic length from the vortex core hosting the first Majorana mode [23]. Therefore if the magnetic length is less than the system size then the vortex and edge states do not interact with each other. Otherwise, when magnetic length exceeds the system size the second Majorana mode is localized on the boundaries.

Nevertheless, the concept of such edge-vortex correspondence breaks in HOTSCs. Since the edge spectrum of HOTSC must be gapped it is natural to expect the gapped excitations of vortex states from the point of view of FOTSC. Yet, the coexistence of hinges modes and zero modes localized on opposite ends of a vortex line in 3D HOTSC is shown in [24], as well as vortex and corner modes have been found simultaneously in a system with the space group $P4/nmm$ in the presence of superconductivity and antiferromagnetic ordering [25]. Moreover, it has been proposed that bulk-vortex correspondence should be considered to predict existence of zero vortex modes in HOTSCs [26].

It should be noted that there are proposals of realization of HOTSC state in $FeTe_{0.55}Se_{0.45}$ [27, 28], that is usually considered as FOTSC [29–31]. There is experimental evidence that helical hinge modes are realized in $FeTe_{0.55}Se_{0.45}$ [32]. Moreover, this compound is an ideal platform to experimentally study the zero energy vortex modes [31], since the ratio of square of superconducting gap and Fermi energy, which characterize the energy of vortex-localized Caroli–de Gennes–Matricon states, is high (an order of $100\ \mu eV$) enough to resolve zero energy modes by STM. Thus, the problem of coexistence of vortex modes and corner or hinge modes in HOTSCs might also be considered experimentally.

In the present study we describe the interplay of double vortex modes and corner modes in the 2D model of HOTSC describing an interface between a two-band normal layer with spin-orbit interaction and a superconducting layer. Usually, a normal layer is considered as a topological insulator with gapped bulk spectrum and gapless edge spectrum [33, 34]. Superconducting pairings can induce a Dirac mass in the edge spectrum and support formation of HOTSC state [35]. As it will be shown in the present study the vortex modes are also gapped in such regime. Therefore, we focus on the case when the normal layer has one or two Dirac cones in the bulk spectrum. In this case superconducting pairings induce a gap both in the bulk and edge spectra and also lead to formation of HOTSC state. The difference from the pre-

vious case here is that such regime supports formation of single or double vortex-localized modes with zero energy that coexist with corner modes.

II. HIGHER-ORDER TOPOLOGICAL SUPERCONDUCTING PHASE

To investigate the possibility of vortex zero modes appearance in HOTSC we consider the two-level Hamiltonian with spin-orbit interaction and singlet superconducting coupling [33]

$$H = \sum_{f\eta\sigma} (\eta\Delta\varepsilon - \mu) \, c_{f\eta\sigma}^\dagger c_{f\eta\sigma} \qquad (1)$$

$$+ \sum_{\eta} \eta \left(\sum_{\langle fm\rangle_x,\sigma} t_x + \sum_{\langle fm\rangle_y,\sigma} t_y + \sum_{\langle\langle fm\rangle\rangle,\sigma} t_1 \right) c_{f\eta\sigma}^\dagger c_{m\eta\sigma}$$

$$+ i\lambda \sum_{\langle fm\rangle} \left[\hat\tau^{\alpha\beta}, e_{fm}\right]_z \hat\sigma_x^{\nu\eta} c_{f\nu\alpha}^\dagger c_{m\eta\beta}$$

$$+ \left(\Delta_x \sum_{\langle fm\rangle_x,\eta} + \Delta_y \sum_{\langle fm\rangle_y,\eta} \right) c_{f\eta\uparrow}^\dagger c_{m\eta\downarrow}^\dagger$$

$$+ \Delta_0 \sum_{f\eta} c_{f\eta\uparrow}^\dagger c_{f\eta\downarrow}^\dagger + \text{H.c.},$$

where $c_{f\eta\sigma}$ annihilates an electron with a spin σ on an A, B orbital (with $\eta = \pm 1$ correspondingly) at a square lattice site $f = (i, j)$; $i, j = 1, ..., N$; $\Delta\varepsilon$ is an on-site energy shift opposite for different orbitals; μ is a chemical potential. The intraorbital nearest-neighbor $t_{x,y}$ as well as next-nearest-neighbor t_1 hopping parameters are of opposite signs for different orbitals leading to the inverted bands. The parameter λ defines an intensity of the interorbital Rashba spin-orbit coupling; e_{fm} is a unit vector pointing along the direction of electron motion from the mth to fth site. The parameters $\Delta_{0,x,y}$ are intensities of the intraorbital on-site and intersite singlet pairing that results in overall $s_\pm$-wave superconductivity in the case $\Delta_x = \Delta_y$ or $s + d_{x^2-y^2}$-wave superconductivity in the case of $\Delta_x = -\Delta_y$. The Pauli matrices $\hat\sigma_n$ and $\hat\tau_n$ ($n = x, y, z$) act in orbital and spin subspaces, respectively.

The elementary excitations of the Hamiltonian (1) can be classified by spin projections number σ and may be written in the form

$$\alpha_\sigma = \sum_f \left[u_{f\sigma} c_{fA\sigma} + v_{f\overline\sigma} c_{fB\overline\sigma} + w_{f\overline\sigma} c_{fA\overline\sigma}^\dagger + z_{f\sigma} c_{fB\sigma}^\dagger \right]. \qquad (2)$$

The bulk spectrum of the system in superconducting

and nonsuperconducting regime is defined as

$$\varepsilon_{sc} = \sqrt{(\varepsilon_{nosc} \pm \mu)^2 + |\Delta_k|^2}, \qquad (3)$$

$$\varepsilon_{nosc} = \sqrt{t_k^2 + |\lambda_k|^2},$$

$$t_k = \Delta\varepsilon + 2t_x \cos k_x + 2t_y \cos k_y + 4t_1 \cos k_x \cos k_y,$$

$$\Delta_k = \Delta_0 + 2\Delta_x \cos k_x + 2\Delta_y \cos k_y,$$

$$\lambda_{k\sigma} = 2\lambda \left(\sin k_y - i\sigma \sin k_x \right),$$

This model is known to provide higher-order topological phase. In the case $\text{sign}(\Delta_x\Delta_y) = -\text{sign}(t_xt_y)$ and $t_1 \neq 0$ or $\Delta\varepsilon \neq 0$ this model supports topological corner states, induced by the change of the effective mass of edge states at the corners [33–35].

In the case of $t_1 = \Delta\varepsilon = 0$ (as it will be discussed in the next section, zero-energy vortex modes can exist in such case) the procedure of defining the effective mass of edge states, carried out previously, is not available, as the nonsuperconducting bulk spectrum is not gapped any more. On the other hand it is obviously that HOTSC phase must be preserved, since the bulk in (3) and edge superconducting spectrum remain gapped at $t_1 = \Delta\varepsilon = 0$ (see [34, 35]). To prove the presence of HOTSC phase in this case one can calculate the polarization of the Wannier bands and the quadrupole (the details of the procedure can be found in [36] and supplementary materials of [8]), which are the bulk topological indexes and cannot be changed, until the superconducting bulk gap or Wannier bands gap closes. The numerical calculation in the case of $|t_x| = |t_y|$, $\Delta_x = -\text{sign}(t_xt_y)\Delta_y$; $\mu, \Delta\varepsilon \to 0$; $t_1, \Delta_0 = 0$ shows the Wannier band polarization to be $(p_x^{\nu_y^-}, p_y^{\nu_x^-}) = (1/2, 1/2)$ along with quadrupole $q_{xy} = 2p_x^{\nu_y^-} p_y^{\nu_x^-} = 1/2$ corresponding to the HOTSC phase. At $|\Delta_0| > |\Delta_x + \text{sign}(t_xt_y)\Delta_y|$ these indexes become trivial $(p_x^{\nu_y^-}, p_y^{\nu_x^-}) = (0, 0)$, $q_{xy} = 0$ demonstrating the trivial superconducting phase.

All the parameter space of the system, which is not separated from the specified nontrivial point by the mentioned above gaps closure, corresponds to the HOTSC phase providing topological corner excitations. In general, there is a combination of two different mechanisms of HOTSC phase destruction. The first is defined by the superconducting coupling constants: if one starts from the noticed before nontrivial point and increases the Δ_0 or changes the ratio Δ_x/Δ_y, then one of the gaps (bulk or Wannier bands gap depending on the specific parameters) will close and reopen at critical value (for $\Delta\varepsilon = \mu = t_1 = 0$ it is $|\Delta_0| = |\Delta_x + \text{sign}(t_xt_y)\Delta_y|$) and the system turns into a trivial superconductor. On the other hand, increasing μ leads to the crossing of the Fermi contour and Δ_k nodal lines turning the system into the nodal phase (for the parameters taken at the noticed above nontrivial point it happens at $|\mu| = 2\sqrt{2}|\lambda|$). The exemplifying phase diagram for the investigated system, obtained with numerical calculations of the bulk band gap and topological indexes is depicted on the Fig.1(a).
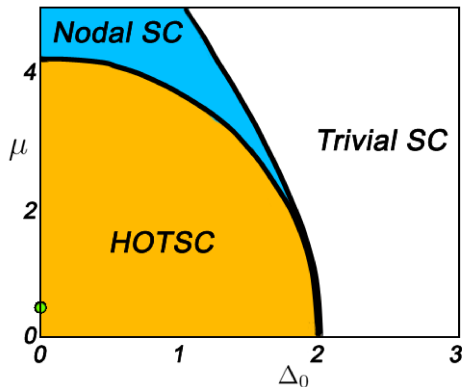
III. ZERO-ENERGY VORTEX MODES

FIG. 1. The topological phase diagram in variables chemical potential μ - on-site superconducting coupling constant Δ_0 for the 2D second-order topological superconductor (1). Parameters are $\Delta\varepsilon = t_1 = 0$, $t_x = -t_y = 2$, $\Delta_x = \Delta_y = 0.5$, $\lambda = 1.5$.

To introduce the superconducting vortex we use the modification of the superconducting coupling parameters with the notation:

$$\Delta_{fm}(\mathbf{r}) = \Delta_{fm} \exp\left(il \arg\left[z(\mathbf{R}_f) - z(\mathbf{R}_m)\right]\right) \cdot \quad (4)$$
$$\cdot \tanh\left(\frac{|\mathbf{R}_f + \mathbf{R}_m - 2\mathbf{R}_v|}{2\xi}\right),$$

where $z(\mathbf{R}) = x+iy$, ξ is coherence length, $l = \pm 1$ for vortex/antivortex, and the vortex is set at the position $\mathbf{R}_v$. While we use this notation for numerical calculations, the analytical approach demonstrates, that the precise form of the superconducting coupling modification does not matter as long, as it is centrally symmetric vortex-like.

We start our investigation of the zero-energy vortex modes with the case of $\Delta\varepsilon = t_1 = 0$ along with $|t_x| = |t_y| = t$. This case corresponds to the gapless bulk energy spectrum ε_{nosc} in (3) in the absence of superconducting coupling with gap closure at the pair of high-symmetry points: $(0,0)$, (π,π) or $(0,\pi)$, $(\pi,0)$ for $\tau = \text{sign}(t_x t_y) = \mp 1$ correspondingly, which are the nodal points of the spin-orbit interaction.

To obtain the zero-energy vortex modes solution for the chosen parameters we use the wide-used procedure [17, 19, 20, 37–39] with one difference: the investigated system is two-level in our case. We make the expansion of the energy terms in Eq. (3) in the vicinity of the spin-orbit interaction nodal points

$$t_k \approx t\,\text{sign}(t_x)c_x(k_y^2 - k_x^2) \quad (5)$$
$$\lambda_{k\sigma} \approx -2\lambda c_x(\tau k_y + i\sigma k_x),$$
$$\Delta_k \approx \Delta_0 + 2c_x(\Delta_x - \Delta_y \tau). \quad (6)$$

with $c_x = \cos k_x^{(N)} = \pm 1$ referring to different nodal points. Obviously that $\tau = -c_x c_y$ with $c_y = \cos k_y^{(N)}$.

As the spectrum is linear in quasi-momentum $\mathbf{k}$ around the nodal points we as a first step neglect the quadratic terms in t_k and Δ_k. We use the continuum approximation $(k_x, k_y) \to -i(\partial_x, \partial_y)$ (with distances, measured in the parameter of the unit cell), and include the modification of superconducting coupling to describe the vortex

$$\Delta_k \to \chi\Delta(r)\exp(il\phi),\ \Delta(r\to\infty)>0,\ \chi=\pm 1. \quad (7)$$

Here (r,ϕ) are polar coordinates with the origin at the center of the vortex, and we separate out the sign of the coupling constant at the nodal point by introduction of χ. As we are interested in zero-energy modes the final equations on coefficients (2) take the form

$$\begin{bmatrix} -\mu & \lambda_{r\sigma} & \sigma\Delta_{r\phi}^* & 0 \\ -\lambda_{r\sigma}^* & -\mu & 0 & -\sigma\Delta_{r\phi}^* \\ \sigma\Delta_{r\phi} & 0 & \mu & \lambda_{r\sigma} \\ 0 & -\sigma\Delta_{r\phi} & -\lambda_{r\sigma}^* & \mu \end{bmatrix} \begin{bmatrix} u_\sigma \\ v_{\overline\sigma} \\ w_{\overline\sigma} \\ z_\sigma \end{bmatrix} = 0,$$

$$\lambda_{r\sigma} = 2\lambda\sigma c_x \exp(-i\sigma\tau\phi)\left(\partial_r - \frac{i\sigma\tau}{r}\partial_\phi\right), \quad (8)$$

$$\Delta_{r\phi} = \chi\Delta(r)\exp(il\phi).$$

As it can be easily checked, these equations separate at $\mu = 0$ into two pairs, which are equivalent up to conjugation along with replacement $\sigma \to \overline\sigma$, which represents that if the α_σ is a zero-energy solution, then $\alpha_\sigma^\dagger$ is also a solution.

The differential equation for $u_\sigma(r,\phi)$, $z_\sigma(r,\phi)$ parameters can be written in the next form

$$\left[\left(\partial_r^2 - \frac{i\sigma\tau}{r^2} + \frac{1}{r^2}\partial_\phi^2\right) - \left(\frac{\Delta(r)}{2\lambda}\right)^2 - \right. \quad (9)$$
$$\left. - \left(\frac{d\Delta(r)/dr}{\Delta(r)} - \frac{1+l\sigma\tau}{r}\right)\left(\partial_r + \frac{i\sigma\tau}{r}\partial_\phi\right)\right]u_\sigma = 0,$$

$$z_\sigma = -2\lambda\chi c_x\Delta(r)\exp(i\phi(l+\sigma\tau))\left(\partial_r + \frac{i\sigma\tau}{r}\partial_\phi\right)u_\sigma.$$

This equation can be solved in the case of $\sigma = -\tau l$ as an exponentially decreasing (increasing) function corresponding to the vortex-localized (boundary-localized) excitation. However, this equations must be accompanied with boundary equations to investigate the fate of the increasing solution. Actually, the system of equations has been extensively studied for FOTSCs [19, 20, 23, 38, 39]. The difference in our case is as follows: Usually it is supposed for FOTSCs that exponentially increasing solutions corresponds to an edge state, localized on the boundary (with exception of [23], where it is localized at finite radius). In HOTSC the edge states are gapped and there is no such a zero mode counterpart. Therefore, there is only a pair of vortex-localized zero-energy excitations in (9) in our case. This solution has the form

$$\begin{bmatrix} u_\sigma \\ z_\sigma \end{bmatrix} = \frac{1}{\sqrt{\mathcal{N}}}\begin{bmatrix} 1 \\ s \end{bmatrix}F(r),\ \ \sigma = -\tau l, \quad (10)$$

$$F(r) = \exp\left(-\int_0^r d\rho\frac{\Delta(\rho)}{2|\lambda|}\right),\ \ s = c_x\chi\,\text{sign}\,\lambda,$$

accompanied with a pair of their hermitian conjugated counterparts (solutions for w_σ and v_σ). It is seen that double zero-energy vortex modes appear due to two distinct nodal points with $c_x = \pm 1$. Previously, the possibility of formation of multiply vortex zero modes was discussed in [39] for crystalline FOTSCs.

One can notice that there is also a mathematical solution with $\sigma = \tau l$.

$$\begin{bmatrix} u_\sigma \\ z_\sigma \end{bmatrix} = \frac{1}{\sqrt{\mathcal{N}}} \begin{bmatrix} \exp(-il\phi) \\ s\exp(il\phi) \end{bmatrix} \frac{F(r)}{r}. \qquad (11)$$

While it has no physical sense at $\mu = 0$, it represents a necessary additive to obtain a solution for $\mu \neq 0$. Making the substitution of the combination of the first solution (10) with a factor $f(r)$ for u_σ, z_σ and the second solution (11) with a factor $g(r)$ for $v_{\overline{\sigma}}$, $w_{\overline{\sigma}}$ (see Appendix A for details) one can obtain the final form

$$\begin{bmatrix} u_\sigma \\ v_{\overline{\sigma}} \\ w_{\overline{\sigma}} \\ z_\sigma \end{bmatrix} = \frac{1}{\sqrt{\mathcal{N}}} \begin{bmatrix} J_0\left(r\mu/2\lambda\right) \\ J_1\left(r\mu/2\lambda\right)\exp(-il\phi) \\ sJ_1\left(r\mu/2\lambda\right)\exp(il\phi) \\ sJ_0\left(r\mu/2\lambda\right) \end{bmatrix} F(r), (12)$$

with $\sigma = -l\tau$. It can be concluded that there are zero energy vortex modes only with one spin projection σ defined by the vortex vorticity sign l. So at finite μ the system still provides two zero-energy vortex-localized excitations and their two hermitian conjugated counterparts, corresponding to two nodal points, at which the nonsuperconducting bulk energy spectrum (3) is gapless.

According to (12) the existence of the zero-energy vortex modes at $\Delta\varepsilon = t_1 = 0$, $|t_x| = |t_y|$ is insensitive to the precise values of spin-orbit interaction λ, chemical potential μ and superconducting couplings $\Delta_{0/x/y}$ (apart from the case of Δ_k to be zero at nodal points), which is confirmed with the numerical calculations.

IV. COEXISTENCE OF ZERO-ENERGY VORTEX AND TOPOLOGICAL CORNER MODES

Now we return to the generalized form of t_k in (3) with unrestricted parameters t_x, t_y, $\Delta\varepsilon$, and t_1, and make the expansion up to quadratic terms in $k_{x,y}$

$$\begin{aligned} t_k &\approx \widetilde{\varepsilon} - tc_x\operatorname{sign}t_x(k_x^2 - k_y^2) - \qquad (13) \\ &- \operatorname{sign}t_x(c_x\delta t - 2t_1\operatorname{sign}t_y)(k_x^2 + k_y^2), \\ \widetilde{\varepsilon} &= \Delta\varepsilon + 2\operatorname{sign}t_x(2c_x\delta t - 2t_1\operatorname{sign}(t_y)), \\ t &= (|t_x| + |t_y|)/2, \quad \delta t = (|t_x| - |t_y|)/2. \end{aligned}$$

The first term $\widetilde{\varepsilon}$ in t_k (13) opens a gap in the spectrum ε_{nosc} at a nodal point and gaps out the vortex modes (12). It is easy to see that size of the gap of the vortex modes $\sim \widetilde{\varepsilon}$. The second term in the continuum limit contains a combination of differential operators, which does not influence on the zero-energy solution (12) due

to its specific dependence on ϕ, justifying neglecting this term previously in Eqs (8) (see Appendix B).

Meanwhile, the effect of the third term is nonzero. Consequently, the vortex modes remain gapless, if both first and third terms in (13) are zero leading to the condition

$$\begin{aligned} t_1 &= c_x\delta t\operatorname{sign}t_y/2, \qquad (14) \\ \Delta\varepsilon &= -2c_x\delta t\operatorname{sign}t_x. \end{aligned}$$

It is seen that for $|t_x| = |t_y| = 0$, $\delta t = 0$ we get $\Delta\varepsilon = t_1 = 0$, the case of which is considered in the previous section.

The parameter ratio (14) represents the condition of appearance of zero-energy vortex modes in the system. To obtain coexistence of topological corner modes and vortex zero modes this condition must be satisfied with the conditions of HOTSC phase formation. As it was mentioned in section II, the necessary condition for the topological corner modes to be realized is $\operatorname{sign}(\Delta_x\Delta_y) = -\operatorname{sign}(t_xt_y) \equiv -\tau$. It should be noted that such restriction is absent for the vortex zero modes. Therefore, if the equality (14) along with $\operatorname{sign}(\Delta_x\Delta_y) = -\tau$ are satisfied, then the coexistence of HOTSC state and zero-energy vortex modes is characterized by the following conditions for the other parameters: 1) chemical potential μ can not lie in the nodal phase (see Fig. 1), where the bulk spectrum ε_{sc} in (3) is gapless and corner, as well as vortex excitations are mixed with the bulk ones (this interval of μ is mainly determined by the spin-orbit coupling parameter λ); 2) we can increase superconducting coupling constant Δ_0 from zero value or change the ratio Δ_x/Δ_y starting from the point $-\tau$ until the bulk or Wannier bands gaps are not close (after reopening one of these gaps the topological corner excitations disappear, as it is seen from the topological phase diagram in Fig. 1, while the vortex zero modes still exist).

The energy spectrum in the presence of corner zero modes and double vortex modes for parameters $\Delta\varepsilon = t_1 = 0$, $t_x = -t_y = 2$, $\Delta_x = \Delta_y = 0.5$, $\lambda = 1.5$, $\Delta_0 = 0$, $\mu = 0.5$ is shown in Fig. 2(a).

It has to be noticed, that in the case of $|t_x| \neq |t_y|$, $\delta t \neq 0$ and satisfying the relations (14) the bulk non-superconducting energy spectrum ε_{nosc} in (3) is gapless only at one nodal point, while the gap at the second nodal point remains finite. Therefore, only single zero-energy vortex mode can exist at $|t_x| \neq |t_y|$. The energy spectrum for this case and parameters $\delta t =$, $\tau = -1$, $\Delta_x = \Delta_y = 0.5$, $\lambda = 1.5$, $\Delta_0 = 0$, $\mu = 0.5$, and t_1, as well as $\Delta\varepsilon$ determined from the relations (14) is presented in Fig. 2(b).

To examine the interaction between corner and vortex zero modes we calculate the spectrum of the finite square-shaped system with different positions of the vortex core: in the bulk, near the edge and near one of the corners. The interaction of the vortex modes with the boundary, when the vortex core is approaching the edge, leads to the appearance of the gap in the vortex modes spectrum
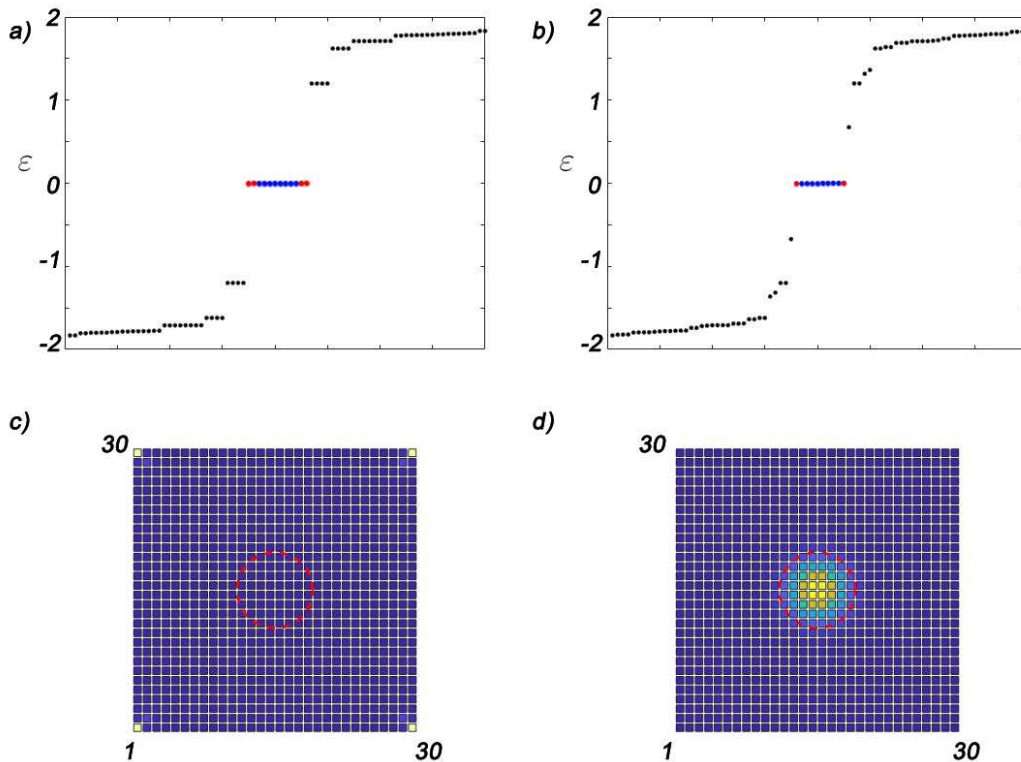
FIG. 2. a) The energy spectrum of the square-shaped system at $\Delta\varepsilon = t_1 = 0$, $t_x = -t_y = 2$, $\Delta_x = \Delta_y = 0.5$, $\lambda = 1.5$, $\mu = 0.5$, $\Delta_0 = 0$ (green point in Fig. 1) with a vortex located at the center of the system and characterizing by $l = 1$, $\xi = 4$. Blue dots correspond to the topological corner modes, red dots — to the vortex zero modes. b) The energy spectrum corresponding to formation of the single vortex mode instead of double vortex modes as in a). Parameters are $t_x = 2$, $t_y = -1.8$; $t_1 = -0.05$ and $\Delta\varepsilon = -0.2$ are obtained from the relation (14), the other parameters are the same as in a). c),d) The corresponding spatial distributions of corner and vortex excitations for the parameters in a), red dashed line depicts the circle of radius ξ around the vortex center.

(Fig.3). Although the spectrum of the vortex modes becomes gapped, the topological corner excitations remain gapless even when the vortex core locates at one of the corners. Similar result is obtained in [24] when a vortex line approaches to hinges of 3D HOTSC.

V. SUMMARY

We investigated the possibility of appearance of zero-energy vortex-localized excitations in the 2D second-order topological superconductor. To obtain the result we used the two-orbital model, which is known to provide topological corner states, with spin-orbit interaction between different orbitals and superconducting coupling with the enhanced s-wave or $s+d_{x^2-y^2}$-wave symmetries.

We analytically demonstrated, that if the bulk energy spectrum in the absence of superconducting coupling is gapless and has Dirac cones, then there can appear one or two zero-energy vortex-localized excitations in the presence of superconductivity, according to the number of the

initial Dirac points. The vortex excitations have only one spin projection defined by the vortex vorticity $l = \pm 1$. Contrary to the first-order topological superconductors, there is no boundary-localized zero-energy counterpart for the vortex-localized modes, as the edge spectrum is gapped.

It was shown that different regimes in the parameter space of the considered model can be realized: HOTSC phase with the only topological corner modes, the region with the only zero-energy vortex modes (double or single), the region of coexistence of such vortex-localized and corner-localized excitations, and the trivial phase where any zero-energy localized excitations are absent. The analytically obtained results were confirmed by the numerical study of the finite-size lattice. The coexistence of the topological corner and zero-energy vortex excitations was shown for the predicted parameters in the case of the vortex core locating away from the boundaries. If the vortex core approaches the boundary, then the vortex-localized excitations become gapped due to their interplay with the boundary modes. Meanwhile, all
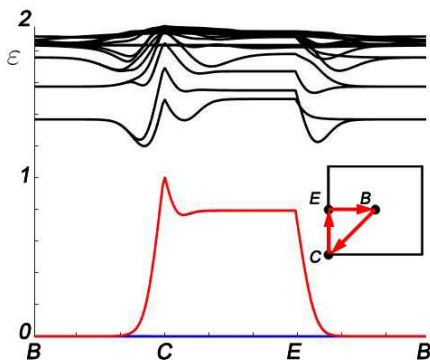
FIG. 3. Dependence of excitation energy of the square-shaped 2D topological superconductor on the vortex position, which moves through the closed path: bulk center (B) → corner (C) → edge center (E) → bulk center. Red line - vortex modes with minimal energy, blue line - topological corner modes.

topological corner excitations remain gapless even in the case of vortex core located at one of the corners.

Appendix A: Zero-energy vortex modes at finite μ

The combination of solutions with allowed r-dependent coefficients for $\sigma = \tau l$ may be written in the form

$$\begin{bmatrix} u_\sigma \\ v_{\overline{\sigma}} \\ w_{\overline{\sigma}} \\ z_\sigma \end{bmatrix} = \frac{1}{\sqrt{\mathcal{N}}} \begin{bmatrix} f(r) \\ g(r)\exp(-il\phi + i\theta) \\ sg(r)\exp(il\phi + i\theta) \\ sf(r) \end{bmatrix} F(r), \quad (\text{A1})$$

Substitution this anzats to (9) reduces them to a pair of equations

$$\partial_r f(r) = \beta g(r), \quad \beta = \frac{\mu}{2\lambda}\tau l c_x \exp(i\theta),$$
$$\partial_r(rg(r)) = -\beta r f(r). \quad (\text{A2})$$

In the case $\mu = 0$ this leads to $f(r) = const$, $g(r) = const/r$. Otherwise this pair of equations reduces to the recurrent relations for Bessel functions

$$\left(\frac{1}{x}\frac{d}{dx}\right)^m [x^n J_n(x)] = x^{n-m} J_{n-m}(x), \quad (\text{A3})$$

with $x = \beta r$, $n = 0, 1$, $m = 1$, if β is real, thus leading to the final form of the zero-energy excitation (12).

Appendix B: Kinetic operators extension

The second term of (13) in the continuum limit contains the differential operator combination

$$(\partial_x^2 - \partial_y^2) = \cos 2\phi \left(\partial_r^2 - \frac{\partial_r}{r} - \frac{\partial_\phi^2}{r^2}\right) + \quad (\text{B1})$$
$$+ 2\frac{\sin 2\phi}{r}\left(\frac{\partial_\phi}{r} - \partial_r \partial_\phi\right).$$

Obviously, due to specific ϕ dependence its effect on zero-energy vortex solutions (12) $\Psi^\dagger(\partial_x^2 - \partial_y^2)\Psi = 0$. Meanwhile the third term

$$(\partial_x^2 + \partial_y^2) = \partial_r^2 + \frac{\partial_\phi}{r} + \frac{\partial_\phi^2}{r^2}, \quad (\text{B2})$$

has no such dependence, thus leading to the finite gap, if it is present in the Hamiltonian.

[1] W. A. Benalcazar, B. A. Bernevig, and T. L. Hughes, Quantized electric multipole insulators, Science **357**, 61 (2017).

[2] J. Langbehn, Y. Peng, L. Trifunovic, F. von Oppen, and P. W. Brouwer, Reflection-symmetric second-order topological insulators and superconductors, Phys. Rev. Lett. **119**, 246401 (2017).

[3] X. Zhu, Tunable majorana corner states in a two-dimensional second-order topological superconductor induced by magnetic fields, Phys. Rev. B **97**, 205134 (2018).

[4] T. Liu, J. J. He, and F. Nori, Majorana corner states in a two-dimensional magnetic topological insulator on a high-temperature superconductor,

Phys. Rev. B **98**, 245413 (2018).

[5] Y. Wang, M. Lin, and T. L. Hughes, Weak-pairing higher order topological superconductors, Phys. Rev. B **98**, 165144 (2018).

[6] Z. Yan, F. Song, and Z. Wang, Majorana corner modes in a high-temperature platform, Phys. Rev. Lett. **121**, 096803 (2018).

[7] G. E. Volovik, Topological superfluid 3 he-b in magnetic field and ising variable, JETP Letters **91**, 201 (2010).

[8] T. E. Pahomi, M. Sigrist, and A. A. Soluyanov, Braiding majorana corner modes in a second-order topological superconductor, Phys. Rev. Research **2**, 032068(R) (2020).

[9] S. B. Zhang, W. B. Rui, A. Calzona, S. J. Choi, A. P. Schnyder, and B. Trauzettel, Topological and holonomic quantum computation based on second-order topological superconductors, Phys. Rev. Research **2**, 043025 (2020).

[10] S. B. Zhang, A. Calzona, and B. Trauzettel, All-electrically tunable networks of majorana bound states, Phys. Rev. B **102**, 100503(R) (2020).

[11] D. A. Ivanov, Non-abelian statistics of half-quantum vortices in p-wave superconductors, Phys. Rev. Lett. **86**, 268 (2001).

[12] J. Alicea, Y. Oreg, G. Refael, F. von Oppen, and M. P. A. Fisher, Non-abelian statistics and topological quantum information processing in 1d wire networks, Nature Physics **7**, 412 (2011).

[13] C. Nayak, S. H. Simon, A. Stern, M. Freedman, and S. DasSarma, Non-abelian anyons and topological quantum computation, Rev. Mod. Phys. **80**, 1083 (2008).

[14] J. Alicea, New directions in the pursuit of Majorana fermions in solid state systems, Rep. Prog. Phys. **75**, 076501 (2012).

[15] A. Stern, F. von Oppen, and E. Mariani, Geometric phases and quantum entanglement as building blocks for non-Abelian quasiparticle statistics, Phys. Rev. B **70**, 205338 (2004).

[16] V. Gurarie and L. Radzihovsky, Zero modes of two-dimensional chiral p-wave superconductors, Phys. Rev. B **75**, 212509 (2007).

[17] J. D. Sau, R. M. Lutchyn, S. Tewari, and S. Das Sarma, Generic New Platform for Topological Quantum Computation Using Semiconductor Heterostructures, Phys. Rev. Lett. **104**, 040502 (2010).

[18] K. Björnson and A. M. Black-Schaffer, Vortex states and Majorana fermions in spin-orbit coupled semiconductor-superconductor hybrid structures, Phys. Rev. B **88**, 024501 (2013).

[19] L. Fu and C. L. Kane, Superconducting Proximity Effect and Majorana Fermions at the Surface of a Topological Insulator, Phys. Rev. Lett. **100**, 096407 (2008).

[20] A. L. Rakhmanov, A. V. Rozhkov, and F. Nori, Majorana fermions in pinned vortices, Phys. Rev. B **84**, 075141 (2011).

[21] C.-K. Chiu, M. J. Gilbert, and T. L. Hughes, Vortex lines in topological insulator-superconductor heterostructures, Phys. Rev. B **84**, 144507 (2011).

[22] A. O. Zlotnikov, Majorana vortex modes in spin-singlet chiral superconductors with noncollinear spin ordering: Local density of states study, Phys. Rev. B **107**, 144513 (2023).

[23] R. S. Akzyanov, A. L. Rakhmanov, A. V. Rozhkov, and F. Nori, Tunable Majorana fermion from Landau quantization in 2D topological superconductors, Phys. Rev. B **94**, 125428 (2016).

[24] M. Kheirkhah, Z. Yan, and F. Marsiglio, Vortex-line topology in iron-based superconductors with and without second-order topology, Phys. Rev. B **103**, L140502 (2021).

[25] Z. Zhang, Z. Wu, C. Fang, F.-c. Zhang, J. Hu, Y. Wang, and S. Qin, Topological superconductivity from unconventional band degeneracy with conventional pairing, Nature Communications **15**, 7971 (2024).

[26] R.-X. Zhang, Bulk-Vortex Correspondence of Higher-Order Topological Superconductors, arXiv:2208.01652 [cond-mat], (2022).

[27] R.-X. Zhang, W. S. Cole, and S. Das Sarma, Helical Hinge Majorana Modes in Iron-Based Superconductors, Phys. Rev. Lett. **122**, 187001 (2019).

[28] R.-X. Zhang and S. Das Sarma, Intrinsic Time-Reversal-Invariant Topological Superconductivity in Thin Films of Iron-Based Superconductors, Phys. Rev. Lett. **126**, 137001 (2021).

[29] D. Wang, L. Kong, P. Fan, H. Chen, S. Zhu, W. Liu, L. Cao, Y. Sun, S. Du, J. Schneeloch, R. Zhong, G. Gu, L. Fu, H. Ding, and H.-J. Gao, Evidence for Majorana bound states in an iron-based superconductor, Science **362**, 333 (2018).

[30] V. Pathak, S. Plugge, and M. Franz, Majorana bound states in vortex lattices on iron-based superconductors, Annals of Physics , 168431 (2021).

[31] T. Machida and T. Hanaguri, Searching for Majorana quasiparticles at vortex cores in iron-based superconductors, Prog. Theor. Exp. Phys. , ptad084 (2023).

[32] M. J. Gray, J. Freudenstein, S. Y. F. Zhao, R. O'Connor, S. Jenkins, N. Kumar, M. Hoek, A. Kopec, S. Huh, T. Taniguchi, K. Watanabe, R. Zhong, C. Kim, G. D. Gu, and K. S. Burch, Evidence for Helical Hinge Zero Modes in an Fe-Based Superconductor, Nano Lett. **19**, 4890 (2019).

[33] Q. Wang, C.-C. Liu, Y.-M. Lu, and F. Zhang, High-temperature majorana corner states, Phys. Rev. Lett. **121**, 186801 (2018).

[34] S. V. Aksenov, A. D. Fedoseev, M. S. Shustin, and A. O. Zlotnikov, Effect of local coulomb interaction on majorana corner modes: Weak and strong correlation limits, Phys. Rev. B **107**, 125401 (2023).

[35] S. V. Aksenov, A. D. Fedoseev, M. S. Shustin, and A. O. Zlotnikov, On the dirac mass of hubbard fermions in strongly correlated higher-order topological superconductor, Physics of the Solid State **65**, 1063 (2023).

[36] W. A. Benalcazar, B. A. Bernevig, and T. L. Hughes, Electric multipole moments, topological multipole moment pumping, and chiral hinge states in crystalline insulators, Phys. Rev. B **96**, 245115 (2017).

[37] T. Fukui, Majorana zero modes bound to a vortex line in a topological superconductor, Phys. Rev. B **81**, 214516 (2010).

[38] R. S. Akzyanov, A. V. Rozhkov, A. L. Rakhmanov, and F. Nori, Tunneling spectrum of a pinned vortex with a robust Majorana state, Phys. Rev. B **89**, 085409 (2014).

[39] S. Kobayashi and A. Furusaki, Double majorana vortex zero modes in superconducting topological crystalline insulators with surface rotation anomaly, Phys. Rev. B **102**, 180505(R) (2020).